High-resolution long-range distributed Brillouin analysis using dual-layer phase and amplitude coding

Yosef London,[1] Yair Antman,[1] Raphael Cohen,[1] Naama Kimelfeld,[1] Nadav Levanon,[2] and Avi Zadok[1,*]

[1]*Faculty of Engineering, Bar-Ilan University, Ramat-Gan 5290002, Israel*
[2]*School of Electrical Engineering, Faculty of Engineering, Tel-Aviv University, Tel-Aviv 6997801, Israel*
[*]*Avinoam.Zadok@biu.ac.il*

Abstract: A new, hybrid time-domain and correlation-domain Brillouin analysis technique is proposed and demonstrated, providing a large number of high-resolution acquisition points. The method is based on dual-layer hierarchal encoding of both amplitude and phase. The pump and signal waves are co-modulated by a relatively short, high-rate binary phase sequence. The phase modulation introduces Brillouin interactions in a large number of discrete and localized correlation peaks along the fiber under test. In addition, the pump wave is also amplitude-modulated by a slower, carefully synthesized, long on-off-keying sequence. Brillouin interactions at the correlation peaks imprint weak replicas of the pump amplitude sequence on the intensity of the output signal wave. The Brillouin amplifications at individual correlation peaks are resolved by radar-like, matched-filter processing of the output signal, following a recently-proposed incoherent compression protocol. The method provides two significant advantages with respect to previous, pulse-gated correlation-domain analysis schemes, which involved a single pump pulse. First, compression of the extended pulse sequence enhances the measurement signal-to-noise ratio, which is equivalent to that of a large number of averages over repeating single-pulse acquisitions. The acquisition times are potentially much reduced, and the number of resolution points that may be practically interrogated increases accordingly. Second, the peak power level of the pump pulses may be lowered. Hence, the onset of phase pattern distortion due to self-phase modulation is deferred, and the measurement range can be increased. Using the proposed method, the acquisition of Brillouin gain spectra over a 2.2 km-long fiber with a spatial resolution of 2 cm is demonstrated experimentally. The entire set of 110,000 resolution points is interrogated using only 499 position scans per choice of frequency offset between pump and signal. A 5 cm-long hot-spot, located towards the output end of the pump wave, is properly recognized in the measurements.

OCIS codes: (290.5900) Scattering, stimulated Brillouin; (060.2370) Fiber optics sensors; (190.2055) Dynamic gratings; (190.4370) Nonlinear optics, fibers.

1. R. W. Boyd, *Nonlinear Optics*, 3rd Edition, (Academic, 2008).
2. A. Zadok, A. Eyal, and M. Tur, "Stimulated Brillouin scattering slow light in optical fibers [Invited]," Appl. Optics **50**(25), E38-E49 (2011).
3. T. Kurashima, T. Horiguchi, and M. Tateda, "Distributed-temperature sensing using stimulated Brillouin scattering in optical silica fibers," Opt. Lett. **15**(18), 1038-1040 (1990).
4. T. Horiguchi, T. Kurashima, and M. Tateda, "A technique to measure distributed strain in optical fibers," IEEE Photonic Tech. L. **2**(5), 352-354 (1990).
5. M. Niklès, L. Thévenaz, and P. A. Robert, "Simple distributed fiber sensor based on Brillouin gain spectrum analysis," Opt. Lett. **21**(10), 758-760 (1996).

#217068 - $15.00 USD Received 15 Jul 2014; revised 17 Oct 2014; accepted 20 Oct 2014; published 24 Oct 2014

6. X. Bao and L. A. Chen, “Recent progress in Brillouin scattering based fiber sensors,” Sensors-Basel **11**(4), 4152-4187 (2011).
7. F. Gyger, E. Rochat, S. Chin, M. Niklès, and L. Thévenaz ,"Extending the sensing range of Brillouin optical time-domain analysis up to 325 km combining four optical repeaters," Proc. SPIE 9157, 23rd International Conference on Optical Fibre Sensors, 91576Q (2014).
8. Y. Peled, A. Motil, and M. Tur, "Fast Brillouin optical time domain analysis for dynamic sensing," Opt. Express **20**(8), 8584-8591 (2012).
9. A. Fellay, L. Thevenaz, M. Facchini, M. Nikles, and P. Robert, "Distributed sensing using stimulated Brillouin scattering : towards ultimate resolution," in 12th International Conference on Optical Fiber Sensors, Vol. **16** of 1997 OSA Technical Digest Series (Optical Society of America, 1997), paper OWD3.
10. Y. Dong, H. Zhang, L. Chen, and X. Bao, "2 cm spatial-resolution and 2 km range Brillouin optical fiber sensor using a transient differential pulse pair," Appl. Optics **51**(9), 1229-1235 (2012).
11. S. M. Foaleng, M. Tur, J. C. Beugnot, and L. Thévenaz, "High spatial and spectral resolution long-range sensing using Brillouin echoes," J. Lightwave Technol. **28**(20), 2993-3003 (2010).
12. K. Hotate and T. Hasegawa, "Measurement of Brillouin gain spectrum distribution along an optical fiber using a correlation-based technique-proposal, experiment and simulation," IEICE T. Electron. **E83-C**(3), 405–412 (2000).
13. Y. Antman, N. Primerov, J. Sancho, L. Thevenaz, and A. Zadok, "Localized and stationary dynamic gratings via stimulated Brillouin scattering with phase modulated pumps," Opt. Express **20**(7), 7807-7821 (2012).
14. Y. Antman, L. Yaron, T. Langer, M. Tur, N. Levanon, and A. Zadok, "Experimental demonstration of localized Brillouin gratings with low off-peak reflectivity established by perfect Golomb codes," Opt. Lett. **38**(22), 4701-4704 (2013).
15. A. Zadok, Y. Antman, N. Primrov, A, Denisov, J. Sancho, and L. Thevenaz, “Random-access distributed fiber sensing,” Laser Photonics Rev. **6**(5), L1-L5 (2012).
16. D. Elooz, Y. Antman, N. Levanon, and A. Zadok, "High-resolution long-reach distributed Brillouin sensing based on combined time-domain and correlation-domain analysis," Opt. Express **22**(6), 6453-6463 (2014).
17. D. Elooz, Y. Antman, and A. Zadok, “Combined time-domain and correlation-domain Brillouin analysis with 1600 meters range and 2 centimeters resolution,” Proc. SPIE 9157, 23rd International Conference on Optical Fibre Sensors, 91576O (2014).
18. K. Song, Z. He, and K. Hotate, "Distributed strain measurement with millimeter-order spatial resolution based on Brillouin optical correlation domain analysis," Opt. Lett. **31**(17), 2526-2528 (2006).
19. R. Cohen, Y. London, Y. Antman, and A. Zadok, “Brillouin optical correlation domain analysis with 4 millimeter resolution based on amplified spontaneous emission,” Opt. Express **22**(10), 12070-12078 (2014).
20. R. Cohen, Y. London, Y. Antman, and A. Zadok, "Few millimeter-resolution Brillouin optical correlation domain analysis using amplified-spontaneous-emission pump and signal waves," Proc. SPIE 9157, 23rd International Conference on Optical Fibre Sensors, 91576B (2014).
21. O. Matsuoka, M. Kishi, and K. Hotate, "Brillouin optical correlation domain reflectometry with double frequency modulation and phase modulation," Proc. SPIE 9157, 23rd International Conference on Optical Fibre Sensors, 91576G (2014).
22. W. Zou, Z. He, and K. Hotate, "Range elongation of distributed discrimination of strain and temperature in Brillouin optical correlation-domain analysis based on dual frequency modulations," IEEE Sens. J. **14**(1), 244-248 (2014).
23. K. Hotate, H. Arai, and K. Y. Song, “Range-enlargement of simplified Brillouin optical correlation domain analysis based on a temporal gating scheme,” SICE J Control, Measurement, and System Integration **1**(4), 271-274 (2008).
24. A. Denisov, M.A. Soto, and L. Thévenaz, "Time gated phase-correlation distributed Brillouin fiber sensor," Proc. SPIE 8794, Fifth European Workshop on Optical Fibre Sensors, 87943I (2013).
25. A. Denisov, M. Soto, and L. Thévenaz," 1’000’000 resolved points along a Brillouin distributed fibre sensor," Proc. SPIE 9157, 23rd International Conference on Optical Fibre Sensors, 9157D2 (2014).
26. N. Levenon and E. Mozeson, *Radar Signals*. New York, (Wiley, 2004).
27. M. Soto, G. Bolognini, and F. Pasquale, "Long-range simplex-coded BOTDA sensor over 120km distance employing optical preamplification," Opt. Lett. **36**(2), 232-234 (2011).
28. M. Soto, X. Angulo-Vinuesa, S. Martin-Lopez, S. Chin, J.D. Ania-Castanon, P. Corredera, E. Rochat, M. Gonzalez-Herraez, and L. Thevenaz, "Extending the real remoteness of long-range Brillouin optical time-domain fiber analyzers," J. Lightwave Technol. **32**(1), 152-162 (2014).
29. M. A. Soto, G. Bolognini, F. Di Pasquale, and L. Thévenaz, "Long-range Brillouin optical time-domain analysis sensor employing pulse coding techniques," Meas. Sci. Technol. **21**(9), 094024 (2010).
30. M. A. Soto, S. Le Floch, and L. Thévenaz, "Bipolar optical pulse coding for performance enhancement in BOTDA sensors," Opt. Express **21**(14), 16390–16397 (2013).
31. M. A. Soto and L. Thévenaz, "Advanced pulse coding techniques for distributed optical fiber sensors," in Frontiers in Optics 2013, I. Kang, D. Reitze, N. Alic, and D. Hagan, eds., OSA Technical Digest (online) (Optical Society of America, 2013), paper FW4I.3.

#217068 - $15.00 USD Received 15 Jul 2014; revised 17 Oct 2014; accepted 20 Oct 2014; published 24 Oct 2014

32. S. Le Floch, F. Sauser, M. Llera, M. A. Soto, and L. Thévenaz, "Colour simplex coding for Brillouin distributed sensors," Proc. SPIE 8794, Fifth European Workshop on Optical Fibre Sensors, 879437 (2013).
33. M. A. Soto, S. Le Floch, and L. Thévenaz, "Bipolar pulse coding for enhanced performance in Brillouin distributed optical fiber sensors," Proc. SPIE 8421, OFS2012 22nd International Conference on Optical Fiber Sensors, 84219Y (2012).
34. N. Levanon, "Noncoherent pulse compression," IEEE T. Aero. Elec. Sys. **42**, 756–765 (2006).
35. D. Kravitz, D. Grodensky, N. Levanon, and A. Zadok,"High-resolution low-sidelobe laser ranging based on incoherent pulse compression," IEEE Photonic Tech. L. **24**(23), 2119-2121 (2012).
36. X. Angulo-Vinuesa, S. Martin-Lopez, P. Corredera, and M. Gonzalez-Herraez, "100 km BOTDA temperature sensor with sub-meter resolution," Proc. SPIE 8421, OFS2012 22nd International Conference on Optical Fiber Sensors, 842117 (2012).
37. X. Angulo-Vinuesa, S. Martin-Lopez, P. Corredera, and M. González-Herraez, "Raman-assisted Brillouin optical time-domain analysis with sub-meter resolution over 100 km," Opt. Express **20**(11), 12147–12154 (2012).
38. M. A. Soto, M. Taki, G. Bolognini, and F. Di Pasquale, "Optimization of a DPP-BOTDA sensor with 25 cm spatial resolution over 60 km standard single-mode fiber using Simplex codes and optical pre-amplification," Opt. Express **20**(7), 6860–6869 (2012).
39. M. Taki, M. A. Soto, G. Bolognini, and F. Di Pasquale, "Study of Raman amplification in DPP-BOTDA sensing employing simplex coding for sub-mtere scale spatial resolution over long fiber distances," Meas. Sci. Technol. **24**(9), 094018 (2013).
40. Y. Antman, N. Levanon, and A. Zadok, "Low-noise delays from dynamic Brillouin gratings based on perfect Golomb coding of pump waves," Opt. Lett. **37**(24), 5259-5261 (2012).
41. S. W. Golomb, "Two-valued sequences with perfect periodic autocorrelation," IEEE T. Aero. Elec. Sys. **28**, 383-386 (1992).
42. N. Levanon, "Cross-correlation of long binary signals with longer mismatched filters," IEE P-Radar Son. Nav. **152**(6), 377–382 (2005).
43. R. Ferguson, private communication, unpublished (2008).
44. A. Zadok, E. Zilka, A. Eyal, L. Thevenaz, and M. Tur, "Vector analysis of stimulated Brillouin scattering amplification in standard single-mode fibers," Opt. Express **16**(26), 21692-21707 (2008).
45. D. Grodensky, D. Kravitz, N. Arbel, N. Levanon, and A. Zadok, "Incoherent pulse compression in laser range finder", Proc. SPIE 9080, Laser Radar Technology and Applications XIX and Atmospheric Propagation XI, 90800M (2014).
46. M. A. Soto and L. Thévenaz, "Modeling and evaluating the performance of Brillouin distributed optical fiber sensors," Opt. Express **21**(25), 31347-31366 (2013).

1. Introduction

Stimulated Brillouin scattering (SBS) is a non-linear effect which can couple between two optical waves along standard optical fibers. In SBS, a relatively intense pump wave interacts with a counter-propagating, typically weaker signal wave, which is detuned in frequency [1]. Effective coupling, however, requires that the difference between the two optical frequencies should closely match a particular, fiber-dependent value known as the *Brillouin frequency shift* $\nu_B \sim 11$ GHz (for standard single mode fibers and at ~1550 nm wavelength). The power of a signal wave whose optical frequency is ν_B below that of the pump is amplified by SBS [1-2]. The value of ν_B varies with both temperature and mechanical strain [3]. Hence, a mapping of the local Brillouin gain spectrum along standard fibers is being used in distributed sensing of both quantities for 25 years [4-6]. Much effort is being dedicated to increasing the range and the number of interrogated points of high-resolution SBS analysis, driven by structural health monitoring applications in the civil engineering, construction, aerospace and transportation sectors.

In Brillouin optical time-domain analysis (B-OTDA), a continuous signal wave is amplified by a pulsed, counter-propagating and intense pump wave, and the output signal power is monitored as a function of time [3-4]. B-OTDA can reach over 300 km range [7], and provide dynamic measurements [8], yet the spatial resolution of the fundamental B-OTDA scheme is restricted to the order of 1 m by the acoustic lifetime τ of approximately 5 ns [9]. Numerous advances have improved the resolution towards cm-scale [6]. In one

#217068 - $15.00 USD Received 15 Jul 2014; revised 17 Oct 2014; accepted 20 Oct 2014; published 24 Oct 2014

demonstration, Dong and coworkers performed a B-OTDA of a 2 km-long fiber with 2 cm resolution [10], and in another Foaleng *et al.* reached 5 cm resolution over 5 km [11].

The complementary technique of Brillouin optical correlation-domain analysis (B-OCDA) relies on the close relation between the spatial profile of the Brillouin interaction and the temporal cross-correlation of the pump and signal complex envelopes [12]. Careful phase or frequency modulation of the two waves confines their correlation to discrete and narrow peaks [12-25]. B-OCDA reached mm-scale resolution [18-20], and over 24,000 resolution points [21]. The range of unambiguous measurements in the basic frequency-modulated B-OCDA was restricted to hundreds of resolution points, due to the simultaneous generation of multiple, periodic correlation peaks. The measurement range was later extended through more elaborate frequency modulation [22]. Increasing the number of interrogated points in both high-resolution B-OTDA and B-OCDA remains difficult, primarily due to low signal-to-noise ratios (SNRs) which mandate averaging over a large number of repeating measurements and long acquisition times.

Recently, we proposed and demonstrated a combined B-OTDA / B-OCDA technique, in which a continuous signal and an amplitude-pulsed pump are both phase-modulated by a short, high-rate binary sequence [16-17]. Due to the short length of the phase code, a large number of correlation peaks are generated during the propagation of the single pump wave pulse. With careful choice of the pump pulse duration with respect to the phase code period and the Brillouin lifetime τ, the SBS amplification which takes place at the different peaks could be temporally resolved in measurements of the output signal power, much like in a B-OTDA [16-17]. The analysis of a 1.6 km-long fiber with 2 cm resolution was demonstrated, using only 127 scans per frequency offset between the pump and signal [17]. Time-gated B-OCDA demonstrations were also reported by Denisov and associates and by Hotate *et al.* [23-25].

While the combined B-OTDA / B-OCDA method reduces the acquisition time of high-resolution B-OCDA considerably, the further increase of its measurement range is rather difficult. Self-phase modulation (SPM) within the intense, isolated pump pulse distorts the underlying phase code, and undermines the spatial confinement of the SBS interaction. Consequently, the acceptable pump power and the resulting measurement SNR both decrease with range. A possible alternative could be the transmission of extended sequences of weaker pump pulses, overlaying the high-rate phase sequence. SBS amplification at each correlation peak would imprint a weak replica of the pump amplitude coding sequence onto the magnitude of the output signal. A matched-filtering process may then be used to compress the multiple replicas into a set of discrete and narrow peaks, with reduced sidelobes [26]. The principle is inspired by pulse compression that is prevalent in radar systems, and is also being successfully employed in ultra-long-reach B-OTDA setups [27-33].

Herein, we report a hybrid B-OTDA / B-OCDA scheme, implementing two layers of hierarchal encoding. In similarity to our earlier work [16-17], both pump and signal are modulated by a relatively short, high-rate binary phase code, introducing multiple narrow correlation peaks. However, rather than using a single pump pulse, the amplitude of the pump wave is modulated by a slower, on-off keying sequence. We employ an incoherent compression protocol, in which binary phase codes of ultra-low sidelobes are converted to unipolar representations that are used in the pump wave modulation [34]. Incoherent compression retains the superior sidelobe suppression of the original phase sequences, even though simple, direct detection of the output signal intensity is carried out [34]. A 1112 bits-long, maximum peak-to-sidelobe (MPSL) sequence was employed in this work. The peak-to-sidelobe ratio of the incoherently compressed sequence in ideal noise-free conditions is as low as -52 dB [35]. The incoherent compression protocol was successfully utilized in laser range-finder measurements at low SNRs [35].

The proposed, dual-coding technique scheme provides a substantial benefit in SNR. The processing gain of a single acquisition trace following sequence compression yields a SNR

#217068 - $15.00 USD Received 15 Jul 2014; revised 17 Oct 2014; accepted 20 Oct 2014; published 24 Oct 2014

that is comparable with that of many averages over repeating, single-pulse acquisitions. This advantage can be leveraged in two ways. Firstly, acquisition times, already reduced by a factor of several hundreds in the combined B-OTDA / B-OCDA configuration [16-17, 25], may be substantially reduced even further. Second, the peak power level of pump pulses may be lowered. The confinement of the SBS interaction to narrow correlation peaks would therefore become less susceptible to SPM, and the measurement range may be extended accordingly. Note that the extension of earlier work is based entirely on more elaborate signal encoding and processing, and does not require any additional fiber-optic components.

The acquisition of the Brillouin gain spectra over a 2.2 km-long fiber with 2 cm resolution was experimentally demonstrated using the proposed dual-hierarchy coding scheme. The entire set of 110,000 resolution points was interrogated using only 499 scans of the correlation peaks positions, per choice of frequency offset between pump and signal. A 5 cm-long hot-spot, located towards the output end of the pump wave, was successfully identified in the measurements. The uncertainty in the reconstructed local values of ν_B is estimated as ±2 MHz. The results demonstrate the potential benefits of using both phase and amplitude coding in distributed Brillouin sensing, and represent the largest set of acquisition points interrogated in high-resolution B-OCDA. Although previous setups successfully demonstrated the potential of reaching over a million points [24,25], only a fraction of the set of potential resolution points could be interrogated within a practical experimental duration. Even larger numbers of resolution points were successfully interrogated in Brillouin fiber sensors that do not involve correlation-domain analysis [7,36-39], with tens of cm resolution.

The remainder of this paper is organized as follows: The principle of operation of dual-hierarchy-encoded, hybrid B-OTDA / B-OCDA is described in section 2. Experimental results are provided in section 3, and a concluding discussion is given in section 4.

2. Principle of operation

2.1. Hybrid B-OTDA / B-OCDA with dual-layer hierarchal encoding

For the purpose of better focus and clarity, we use the previously presented analysis of the hybrid B-OTDA / B-OCDA protocol as a starting point for the following description [16]. The reader is referred to that work, and to the earlier introduction of phase coding-based B-OCDA [13,15], for greater detail. The complex magnitude of the acoustic density fluctuations in fiber position z and at time t is given by [13]:

$$Q(t,z) = jg_1 \int_0^t \exp\left[-\Gamma_A (t-t')\right] A_p\left(t' - \frac{z}{v_g}\right) A_s^*\left[t' - \frac{z}{v_g} + \theta(z)\right] \mathrm{d}t' \qquad (1)$$

In Eq. (1), g_1 is an electro-strictive parameter of the fiber, v_g is the group velocity of light in the fiber, $A_p(t)$ denotes the instantaneous complex envelope of the SBS pump wave entering the fiber at $z=0$ and propagating in the positive z direction, and $A_s(t)$ denotes the complex envelope of the counter-propagating signal wave which enters the fiber at $z=L$. The position-dependent temporal offset $\theta(z)$ is defined as: $\theta(z) \equiv (2z-L)/v_g$. The bandwidth Γ_A is given by the angular frequency offset $\Omega = 2\pi\nu$ between the central optical frequencies of pump and signal, and by the local value of the Brillouin shift $\Omega_B(z) = 2\pi\nu_B(z)$: $\Gamma_A(\nu,z) \equiv j\left[\left(\Omega_B^2(z) - \Omega^2 - j\Omega\Gamma_B\right)/2\Omega\right]$. It reduces to half the Brillouin linewidth: $\Gamma_A = \frac{1}{2}\Gamma_B = 1/(2\tau)$, when $\Omega = \Omega_B(z)$.

The signal envelope at its point of entry into the fiber is modulated by a phase sequence c_n, with a symbol duration T_{phase} that is much shorter than the acoustic lifetime τ:

#217068 - $15.00 USD Received 15 Jul 2014; revised 17 Oct 2014; accepted 20 Oct 2014; published 24 Oct 2014

$$A_s\left(z=L,t\right)=A_{s0}\sum_n c_n \mathrm{rect}\left[\frac{t-nT_{phase}}{T_{phase}}\right]\equiv A_s\left(t\right) \tag{2}$$

Here A_{s0} is a constant magnitude, c_n is a phase code of unity magnitude that is repeated every N_{phase} symbols, and $\mathrm{rect}(\xi)$ equals 1 for $|\xi|\le 0.5$ and zero elsewhere [40]. A short, perfect Golomb code is used in the phase modulation [41]. The special cyclic auto-correlation properties of these codes help reduce the noise due to residual off-peak reflectivity considerably. The implementation of Golomb codes in Brillouin interactions was discussed in detail elsewhere [14,40]. The phase of the pump wave is modulated by the same sequence. In addition, the amplitude of the pump wave is also modulated by a second binary sequence of length N_{amp} and symbol duration T_{amp} :

$$A_p\left(z=0,t\right)=A_{p0}\sum_{m=1}^{N_{amp}} d_m \mathrm{rect}\left(\frac{t-mT_{amp}}{T_{amp}}\right)\times\sum_n c_n \mathrm{rect}\left[\frac{t-nT_{phase}}{T_{phase}}\right]\equiv A_p\left(t\right) \tag{3}$$

In Eq. (3), A_{p0} is a constant magnitude and d_m assume binary values of 1 or 0 according to the sequence design. The symbol durations of the phase and amplitude sequences are chosen so that $\frac{1}{2}N_{phase}T_{phase}>T_{amp}>\tau$.

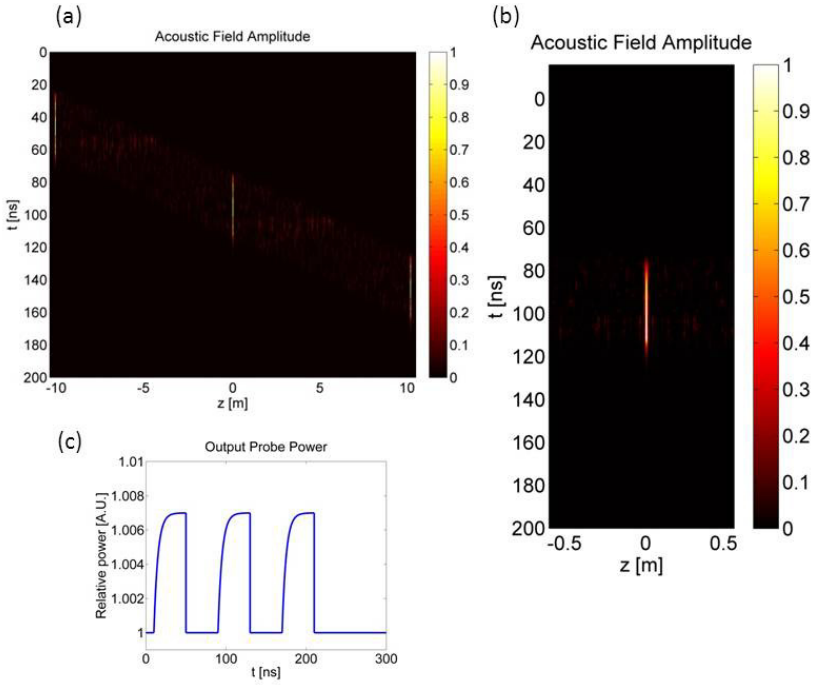

Fig. 1. (a) - Simulated magnitude of the acoustic wave density fluctuations (in normalized units), as a function of position and time along a 20 m-long fiber section. Both pump and signal waves are co-modulated by a repeating perfect Golomb phase code that is 499 bits long, with symbol duration of 200 ps. The pump wave is further modulated by a single amplitude pulse of 40 ns duration (see Eq. (2) and Eq. (3)). The acoustic field, and hence the SBS interaction between pump and signal, is confined to three discrete and periodic narrow correlation peaks within the simulated section. The peaks are built up sequentially one after another with no temporal overlap [16-17]. (b) – Magnified view of the acoustic wave magnitude in the central 1 m of the simulated fiber. (c) - Simulated output signal power as a function of time. The trace consists of a series of three isolated amplification events, each of which can be unambiguously related to the SBS interaction at a specific correlation peak of known location.

#217068 - $15.00 USD Received 15 Jul 2014; revised 17 Oct 2014; accepted 20 Oct 2014; published 24 Oct 2014

Figure 1(a) shows a numerical calculation of the acoustic field magnitude $Q(t,z)$ using Eq. (1), subject to the boundary conditions of Eq. (2) and Eq. (3). A magnified view of $Q(t,z)$ at the center of the simulated fiber is shown in Fig. 1(b). First, the pump wave is restricted to a single amplitude pulse, as in previous works [16-17,25]. The calculation parameters were $T_{phase} = 200$ ps, $N_{phase} = 499$, and $T_{amp} = 40$ ns. The acoustic field is confined to a discrete set of spatially-periodic correlation peaks, whose width $\Delta z = \frac{1}{2} v_g T_{phase}$ equals 2 cm in this case. The separation between neighboring peaks is $N_{phase} \cdot \Delta z$. The temporal duration of each correlation peak is restricted to the order of T_{amp}, hence the peaks do not overlap in the time domain. Figure 1(c) shows the simulated output signal power as a function of time: $\left|A_s(z=0,t)\right|^2$. The trace consists of a series of isolated amplification events, each of which can be unambiguously related to the SBS interaction at a specific correlation peak of known location [16-17]. The locations of the correlation peaks can be offset in Δz increments with proper retiming of the phase modulation of the pump and signal [13,15]. The correlation peaks would return to their initial locations every N_{phase} steps, hence N_{phase} scans for each choice of ν would be sufficient for the mapping of the Brillouin gain spectra over the entire length of the fiber under test.

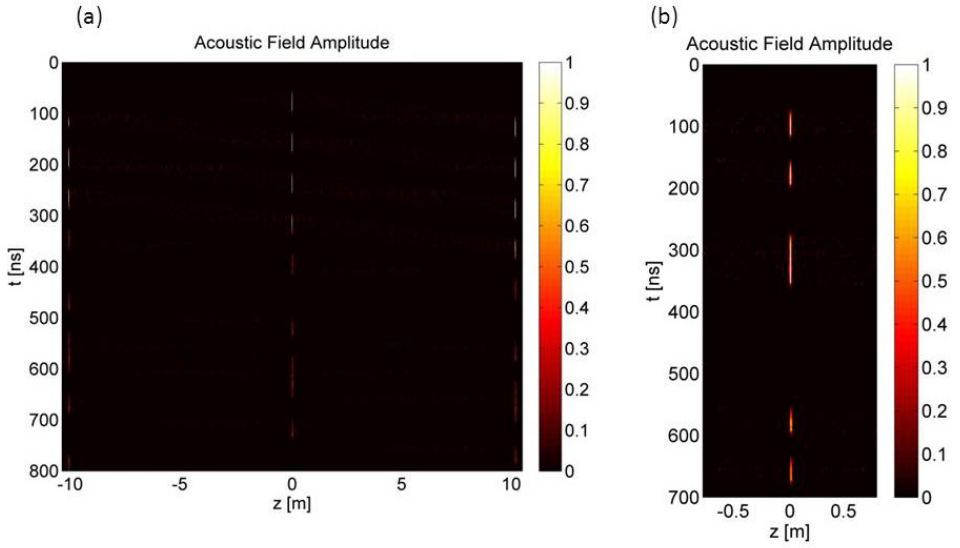

Fig. 2: (a) - Simulated magnitude of the acoustic wave density fluctuations (in normalized units), as a function of position and time along a 20 m-long fiber section. Both pump and signal waves are co-modulated by a repeating perfect Golomb phase code that is 499 bits long, with symbol duration of 200 ps. The pump wave is further modulated by a 26 bits-long amplitude sequence, with a pulse duration of 40 ns. The acoustic field at the three correlation peaks of the phase codes is turned on and off by the overlaying amplitude modulation of the pump wave. (b) - Magnified view of the acoustic wave magnitude in the central 1 m of the simulated fiber.

Consider next the extension of Fig. 1 to the amplitude modulation of the pump wave by a binary sequence of N_{amp} pulses. Figure 2(a) shows the calculated magnitude of the acoustic field $Q(t,z)$. A magnified view of the center of the fiber is shown in Fig. 2(b).The parameters of the phase coding and the duration of pump pulses are the same as those of Fig. 1. The 26 bits-long amplitude modulation sequence was drawn from the Barker 13 bipolar sequence,

#217068 - $15.00 USD Received 15 Jul 2014; revised 17 Oct 2014; accepted 20 Oct 2014; published 24 Oct 2014

following a protocol that is discussed in the following subsection. Once again, the acoustic field is spatially confined to the discrete and narrow correlation peaks of the high-rate phase modulation sequence. In contrast to Fig. 1, however, the acoustic field at each correlation peak is switched on and off by the amplitude modulation of the pump wave, on a time scale of T_{amp}. The SBS interaction at each correlation peak therefore contributes a series of amplification events to the output signal wave, which replicates the amplitude modulation pattern of the pump wave.

As an illustration, the simulated contribution of the SBS interaction at a single correlation peak to the output signal wave $\left|A_s\left(z=0,t\right)\right|^2$ is shown in Fig. 3(a). It consists of 13 pulses, corresponding to the 13 bits of the amplitude code for which $d_m=1$. Figure 3(b) shows the compressed form of the output signal sequence. The processed waveform is characterized by a single main peak. With the exception of the two negative lobes at the time slots immediately adjacent to the main peak, the residual sidelobes are strongly suppressed. Sidelobe suppression is the subject of careful sequence synthesis. The post-processing compression protocol and the attributes of the compressed waveform are addressed in detail in the following subsection.

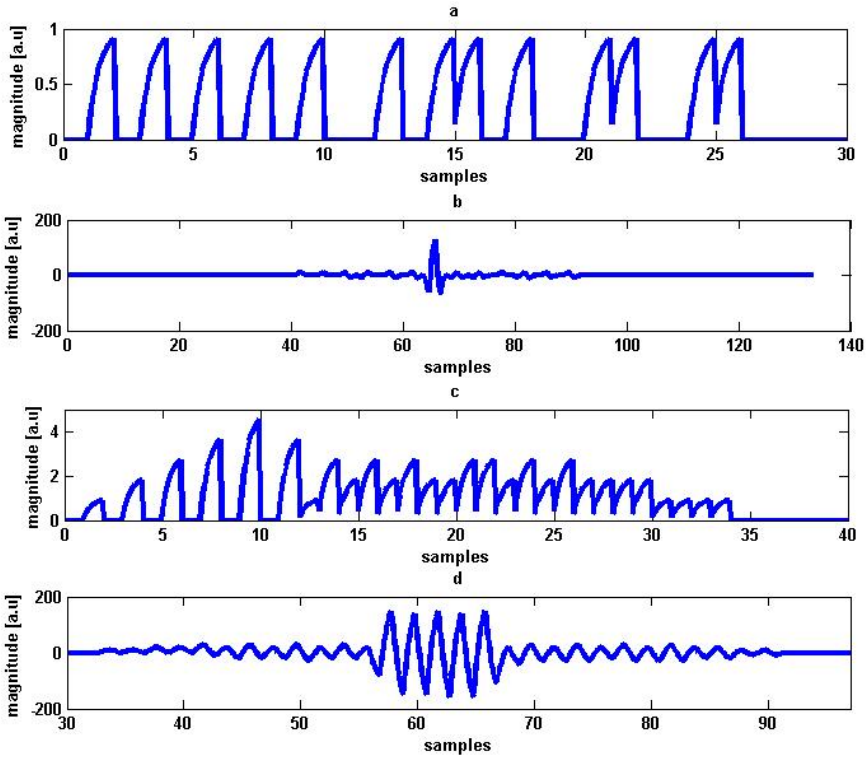

Fig. 3: (a): Simulated intensity of the output signal as a function of time, following SBS interaction at a single correlation peak. Both pump and signal waves are co-modulated by a repeating perfect Golomb phase code that is 499 bits long, with symbol duration of 200 ps. The pump wave is further modulated by a 26 bits-long amplitude sequence, with a pulse duration of 40 ns. 13 amplification events are observed, corresponding to 13 pulses within the amplitude modulating sequence which assume '1' value. (b): Incoherently compressed form of the simulated output signal intensity of the panel (a). (c): Simulated intensity of the output signal as a function of time, following SBS interaction at five adjacent correlation peaks. The modulation of pump and signal is the same as that of panel (a). (d): Incoherently compressed form of the simulated output signal intensity of panel (c), resolving five localized amplification events. In all panels, the horizontal time axis is given in units of the amplitude modulation bit duration.

#217068 - $15.00 USD Received 15 Jul 2014; revised 17 Oct 2014; accepted 20 Oct 2014; published 24 Oct 2014

Figure 3(c) shows the combined contributions of the SBS interactions at five adjacent correlation peaks to the output signal $\left|A_s\left(z=0,t\right)\right|^2$. The five overlapping imprints of the amplitude-modulated pump sequence cannot be separated directly. However, the post-detection processing of the output signal effectively compresses the waveform and recovers five individual amplification events (Fig. 3(d)). As in Fig, 3(b), the favorable correlation properties of the chosen amplitude code lead to an effective suppression of residual off-peak sidelobes.

The multi-peak compressed form of the probe signal in Fig. 3(d) is analogous to that obtained by the previous, single-pulse hybrid B-OTDA / B-OCDA scheme (Fig. 1(c), [16]). However, the magnitude of each compressed peak corresponds to the sum of 13 amplification pulses added together. The SNR of the processed traces may therefore be considerably better than that obtained by a single pump pulse. The improvement in SNR scales with the length of the amplitude sequence. In this work we use a 2224 bit-long sequence, whose duration of ~ 100 μs is on the order of five times of flight back-and-forth along 2 km of fiber. Use of the sequence could yield a SNR improvement by a far larger factor. The hierarchal duel-layer encoding of both phase and amplitude could therefore reduce the acquisition time that is necessary for the construction of Brillouin gain spectra with sufficient fidelity.

2.2. Incoherent pulse compression

In this subsection, the protocol for incoherent pulse compression of amplitude sequences is introduced [34,42]. The majority of pulse compression waveforms known in the literature are constructed using frequency modulation, either linear or nonlinear, or through phase coding (bipolar and poly-phase sequences) [26]. Phase and frequency codes generally provide superior sidelobe suppression, compared with that of amplitude-based or unipolar sequences. However, only the intensity of the output signal wave is measured in our Brillouin analysis setup.

In 2006, Levanon had proposed a novel coding scheme for the effective compression of incoherently detected, unipolar pulse sequences [34]. The unipolar sequences are derived from low-sidelobe, bipolar codes through a pulse-position modulation algorithm [14,34]. Consider a bipolar code of length N: $\tilde{D}_m$, where $m=1\ldots N$. A unipolar code of length $2N$ is generated based on $\tilde{D}_m$ through pulse position modulation: if $\tilde{D}_m=1$, then $d_{2m-1}=1$ and $d_{2m}=0$. For $\tilde{D}_m=-1$, $d_{2m-1}=0$ and $d_{2m}=1$ are chosen instead [34]. The code d_k, $k=1\ldots 2N$, is used to modulate the intensity of the pump wave as described in the preceding subsection. A bipolar matched filtering sequence r_k of length $2N$ is constructed in a similar manner: r_k is set to 1 if $d_k=1$ and equals -1 if $d_k=0$ [34]. The code r_k is digitally stored for post-detection processing. The transmission or measurement of phase information in the optical setup is not required.

As an example, the construction of the d_k and r_k codes corresponding to the Barker 13 bipolar sequence is illustrated in Fig. 4(a). The aperiodic cross-correlation between these two codes is shown in Fig. 4(b), alongside the aperiodic auto-correlation of the original bipolar Barker 13 sequence. With the exception of the two sidelobes immediately adjacent to the main correlation peak, the cross-correlation replicates the sidelobe suppression of the original bipolar code [34]. The two pronounced negative lobes, that are also evident in Fig. 3(b), require that the period of the phase code: $N_{phase}\cdot T_{phase}$, is at least twice as long as the duration of individual amplitude pulses T_{amp}. When this condition is met, the detrimental effect of the negative sidelobes on the recovery of adjacent peaks is mitigated (see Fig. 3(d)).

#217068 - $15.00 USD Received 15 Jul 2014; revised 17 Oct 2014; accepted 20 Oct 2014; published 24 Oct 2014

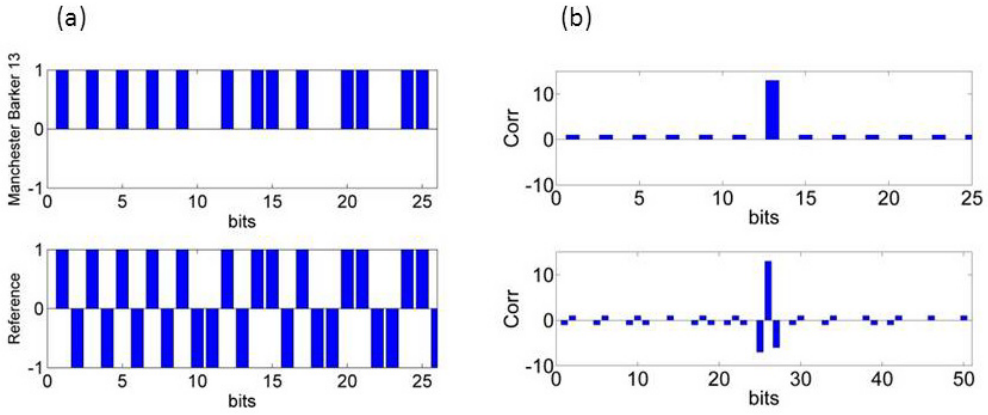

Fig. 4: (a) - Transmitted code *d* (top) and matched filtering code *r* (bottom), corresponding to the Barker 13 code: [1 1 1 1 1 -1 -1 1 1 -1 1 -1 1]. (b) - Top – aperiodic auto-correlation of the Barker 13 bipolar code. The correlation peak is 13, whereas the maximal sidelobe equals unity. Bottom – aperiodic cross-correlation between the transmitted code *d* and matched filtering code *r* corresponding to the Barker 13 bipolar code. With the exception of the two time slots in the immediate vicinity of the central peak, the suppression of sidelobes reaches that of the original bipolar sequence [35].

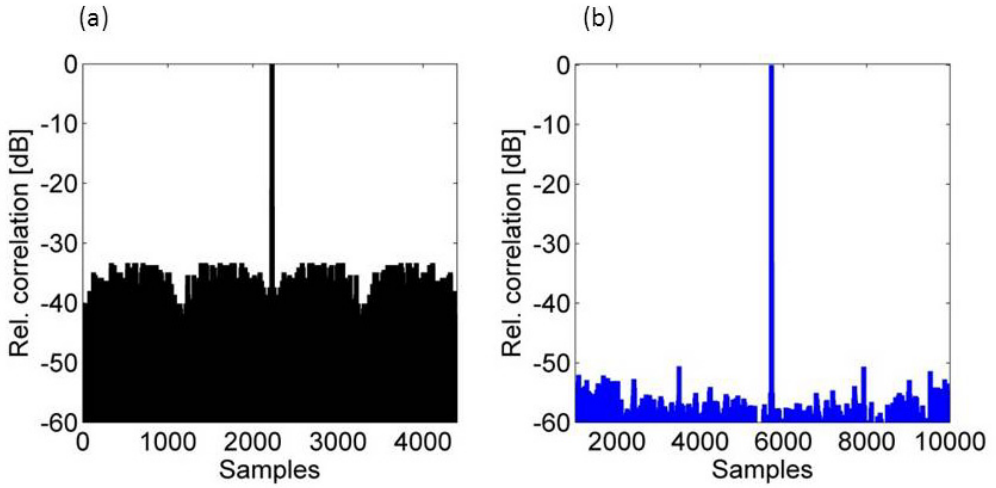

Fig. 5: Calculated incoherent compression of a 1112 pulses-long unipolar sequence. The code was drawn from a 1112 bit-long, bipolar MPSL sequence through a pulse-position modulation algorithm. Both matched (a) and mismatched (b) filters were used in the compression process. [35].

In this work, the SBS interactions at more than 200 correlation peaks are simultaneously interrogated. The compressed main lobe corresponding to each location is in overlap with the sidelobes of all other compressed replicas of the amplitude-modulation sequence. Therefore the choice of sequences having particularly low sidelobes in their aperiodic auto-correlation is essential. The sequence used in this work was constructed from a 1112 bits-long MPSL bipolar code [35, 43], following the pulse position protocol described above. Long codes with low side-lobes of their aperiodic auto-correlation functions can be synthesized through the embedding of one good, short code inside another (see section 6.1.2 in [26]). Figure 5(a) shows the simulated cross correlation between the codes d_k and r_k. The peak-to-sidelobes ratio of the incoherently compressed sequence is -33 dB. The cross-correlation sidelobes can be further suppressed using a mismatched filtering process, in which the sequence r_k is replaced by a code $\tilde{r}_k$ that is three times longer, and whose elements are not restricted to ±1.

#217068 - $15.00 USD Received 15 Jul 2014; revised 17 Oct 2014; accepted 20 Oct 2014; published 24 Oct 2014

Considerable additional suppression of the sidelobes can be obtained, at the cost of a modest degradation in the central correlation peak power [26]. Figure 5(b) shows the mismatch-filtered, incoherently compressed form of the amplitude sequence. The theoretical suppression of sidelobes reaches -52 dB. The incoherent compression of sequences drawn from long bipolar codes was successfully employed in laser ranging measurements [35].

2.3. Self-phase modulation restrictions on the number of acquisition points

SPM could distort the phase modulation pattern of the SBS pump wave. As an order-of-magnitude estimate, we may represent the threshold for SPM-induced distortion as $\gamma\left|A_{p0}\right|^2 L \approx 1$, where γ is the Kerr nonlinearity coefficient of the fiber under test. For standard single mode fibers at 1550 nm wavelength, $\gamma \sim$ 1.3 [W×km]$^{-1}$. The relative SBS power gain of the signal wave, within a single correlation peak and due to a single pump pulse, is therefore restricted to:

$$\frac{\left|A_{s0}\right|^2\left[\exp\left(g_0\left|A_{p0}\right|^2\cdot\Delta z\right)-1\right]}{\left|A_{s0}\right|^2}\approx g_0\left|A_{p0}\right|^2\Delta z\le\frac{g_0}{\gamma}\cdot\frac{\Delta z}{L}=\frac{g_0}{\gamma}\cdot\frac{1}{M}\approx\frac{100}{M} \qquad (4)$$

Here $g_0 \sim$ 100 - 200 [W×km]$^{-1}$ is the SBS gain coefficient of the fiber under test, and $M = L/\Delta z$ is the number of potential resolution points. Consider a single-pulse hybrid B-OTDA / B-OCDA system that is restricted by thermal noise and / or by noise from optical amplification of the signal wave. The SNR of such a system degrades linearly with M, therefore the number of averages over repeating measurements that is necessary to retain a given SNR value scales with M^2. In addition, the duration of a single acquisition trace scales with L. Therefore, for a fixed resolution Δz, the overall acquisition time scales with L^3. The potential SNR enhancement that is provided by the dual-layer hierarchal encoding could be instrumental in relieving the acquisition time bottleneck, which has thus far restricted the number of high-resolution points that could be interrogated in a realistic experiment.

3. Experimental setup and results

Figure 6 shows the experimental setup used in the demonstration of the dual-layer encoding, hybrid B-OTDA / B-OCDA technique. Both the pump and signal waves were drawn from a single laser diode at 1550 nm wavelength. An electro-optic phase modulator at the laser output was driven by an arbitrary waveform generator (AWG), programmed to repeatedly generate a 499 bits-long perfect Golomb phase code with symbol duration of approximately 200 ps. This symbol duration corresponds to a spatial resolution of 2 cm [16-17]. The modulated light was split into pump and signal branches. Light in the pump branch was first amplitude-modulated by a sine wave of radio-frequency ν, in suppressed-carrier format. The value of ν was scanned in increments of δ = 5 MHz. Only the upper modulation sideband was retained by a narrow, tunable optical band pass filter. Pump light was then amplitude-modulated again by the output waveform of a second AWG, programmed to generate the unipolar representation of the 1112 bits-long MPSL sequence with symbol duration of 40 ns. The pump wave was then amplified to an average power of 100 mW by an erbium-doped fiber amplifier. A polarization scrambler was used to prevent polarization-induced fading of the SBS interaction [44].

Light in the signal branch was delayed in a 25 km-long fiber path imbalance, necessary for scanning the positions of the phase-coded correlation peaks as described in detail in [15]. The signal and pump waves were launched into opposite ends of a 2.2 km-long fiber under test. A 5 cm-long hot spot towards the output end of the pump wave was heated to 55°C. The output signal wave was detected by a 200 MHz-wide photo-detector and sampled by a

#217068 - $15.00 USD Received 15 Jul 2014; revised 17 Oct 2014; accepted 20 Oct 2014; published 24 Oct 2014

digitizing oscilloscope. Each trace was averaged over N_{av} = 128 repetitions. The acquired traces were digitally filtered prior to subsequent processing to 50 Msamples/s, in order to reduce the additive noise of the photo-detector. The obtained waveform was compressed using a mismatched filter (see Fig. 5), following the incoherent compression protocol discussed earlier [26,35], and using off-line processing. The procedure was repeated for 20 values of frequency offsets ν, and for 499 positions of the narrow correlation peaks. The net time of flight necessary for the entire experiment was 25 s. The experimental duration was much longer, about 1.5 hours, limited by the latencies of averaging by the sampling oscilloscope and by the switching of instrumentation in a research laboratory environment. These limitations are not fundamental.

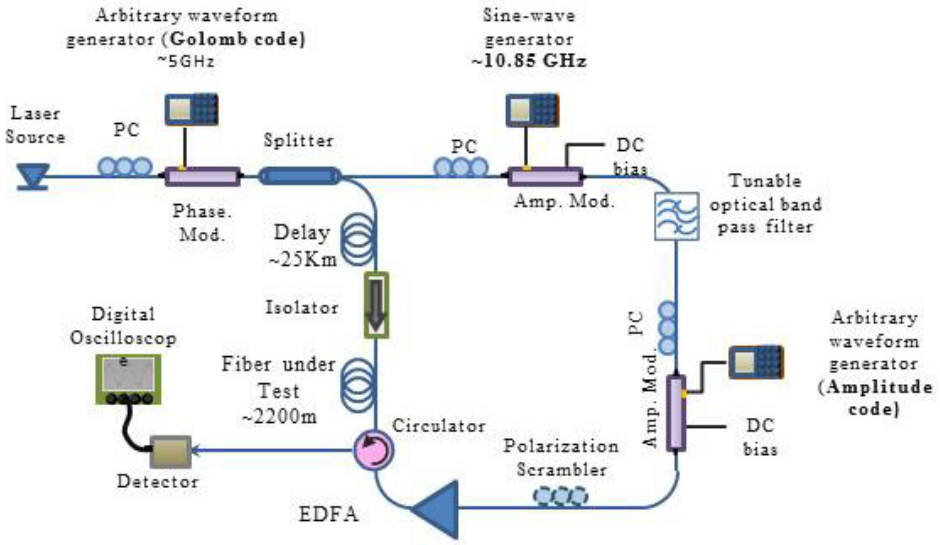

Fig. 6. Experimental setup for hybrid B-OTDA / B-OCDA. EDFA: erbium-doped fiber amplifier. Amp. Mod.: amplitude modulator. Phase Mod.: phase modulator

Figure 7 presents a small fraction of two compressed traces, taken for the same positions of the correlation peaks. Only four peaks out of over 200 are shown for clarity, the final of which is in overlap with the hot spot. The magnitude of each gain event in the traces represents the extent of SBS amplification at a single correlation point of known location (see the simulation results of Fig. 3(d) for comparison). The blue trace was obtained for ν = 10.845 GHz which equals ν_B of the fiber under test at room temperature, whereas the red trace was acquired at the Brillouin shift at the temperature of the hot post (ν = 10.88 GHz). The observed gain at the location of the hot spot is stronger for an offset of 10.88 GHz than for 10.845 GHz. The opposite is true for the other locations.

Figure 8(a) shows the Brillouin gain map as a function of position and ν. The map combines the data of 499 spatial positions of the correlation peaks, covering all 110,000 resolution points along the fiber. The SBS gain spectra at room temperature are centered at ν_B ~ 10.845 GHz and characterized by a full width at half maximum of approximately 30 MHz, in agreement with expectations. Figure 8(b) shows a magnification of the SBS gain map in the vicinity of the hot spot. The region of lower Brillouin frequency shift around 2183.95 m corresponds to the position of a fusion splice.

#217068 - $15.00 USD Received 15 Jul 2014; revised 17 Oct 2014; accepted 20 Oct 2014; published 24 Oct 2014

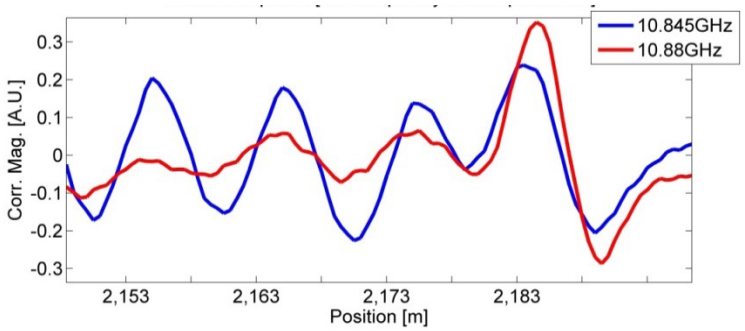

Fig. 7. Examples of experimentally obtained, incoherently compressed traces of the output signal wave, taken for the same location of the phase-code correlation peaks. Only four peaks out of over 200 are shown for clarity. The final peak is in overlap with the hot spot. The blue (red) trace was taken at a frequency offset between pump and signal of 10.845 GHz (10.88 GHz), which corresponds to the Brillouin shift at room temperature (temperature of the hot spot).

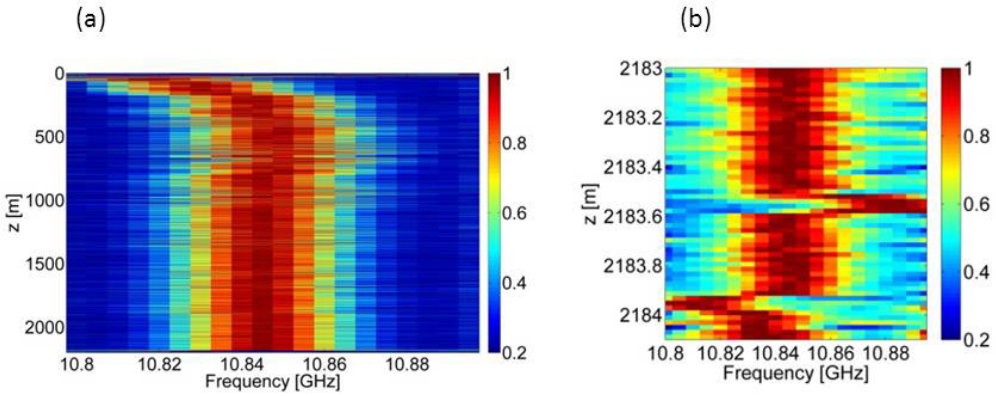

Fig 8. Measured Brillouin gain map (relative units), as a function of frequency offset between pump and signal, and of position along a 2200 m-long fiber under test. A 5 cm-long hot spot was located towards the output end of the fiber. The map was reconstructed using 499 scans per frequency offset. The complete map is shown in the left-hand panel, and a zoom-in on the hot spot region is shown in the right-hand panel.

The reconstructed Brillouin shift as a function of position is shown in Fig. 9(a). The experimental error σ_ν in the reconstructed Brillouin shift is estimated by the standard deviation of the difference $\nu_B(z)-\nu_B(z-\Delta z)$, to be on the order of ±2 MHz. With the exception of the hot spot, it is assumed that any variations in the local Brillouin shift over short segments of length Δz are due to noise, and do not represent physically meaningful strain or temperature changes. Larger variations in $\nu_B(z)$ that are observed in Fig. 9(a) are continuous over tens of cm, and represent actual, periodic strain patterns that are due to the winding of the fiber around a drum. A magnified view of the region including the hot spot is shown in Fig. 9(b). The hot spot and splice are clearly recognized.

#217068 - $15.00 USD Received 15 Jul 2014; revised 17 Oct 2014; accepted 20 Oct 2014; published 24 Oct 2014

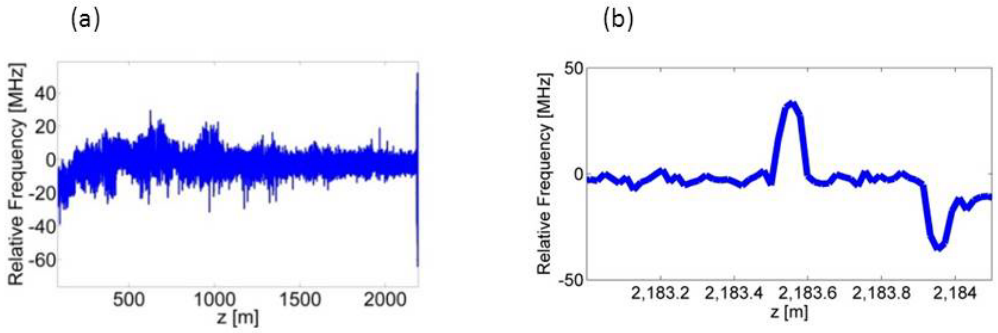

Fig. 9. (a) Brillouin frequency shift (relative to 10.845 GHz) as a function of position, as extracted from the experimental Brillouin gain map of Fig. 8 above. (b) Zoom-in on the hot spot region towards the end of the fiber.

4. Summary and discussion

A novel hybrid B-OTDA / B-OCDA technique was proposed and demonstrated. The method relies on hierarchal dual-layer coding of both phase and amplitude. Phase coding of pump and signal confines the interaction to narrow correlation peaks, whereas the super-imposed amplitude coding of the pump leads to a simultaneous interrogation of multiple peaks with higher SNR. A 499 bits-long perfect Golomb code was used in the phase modulation, chosen for the particularly low sidelobes of its cyclic auto-correlation function. Golomb codes help suppress noise due to residual Brillouin interactions outside the correlation peaks. Amplitude modulation employed the incoherent compression of a unipolar representation of a long MPSL sequence, which is characterized by low sidelobes of its aperiodic auto-correlation function. MPSL sequences reduce the cross-interference in the simultaneous interrogation of hundreds of correlation peaks. The duration of the MPSL sequence exceeded the coherence time of the laser diode source available to us. The finite coherence time of the source might have degraded the suppression of sidelobes. A quantitative study of the effects of source coherence on the performance of the proposed method is beyond the scope of the present work.

The Brillouin gain spectra were experimentally acquired over a 2.2 km-long fiber under test, with a spatial resolution of 2 cm. All 110,000 potential resolution points were interrogated, using only 499 scans of the correlation peaks positions per choice of frequency offset between pump and signal. A 5 cm-long hot spot towards the output end of the fiber was properly recognized in the measurements. The proposed technique could alleviate the need for intense pump pulses, and thereby reduce distortions due to SPM.

Several types of codes could be used in amplitude modulation of the pump wave. For example, the incoherent compression of complementary Golay code pairs, using the same protocol of section 2.2, was successfully employed in laser range-finding experiments [45]. Note that the use of code pairs would require twice the number of scans that is necessary when using a single sequence. The SNR of single-pulse measurements could also be improved, in principle, by simplex coding of the pump wave amplitude, as in coded long-range B-OTDA ([27] and elsewhere). However, simplex coding would require the successive acquisition of the output signal wave, taken for different pump modulation code words, for each position of the correlation peaks and for each value of ν. The overall acquisition time might become prohibitively long.

In a recent work, Soto and Thevenaz proposed the following figure of merit for the evaluation of distributed Brillouin sensor configurations [46]:

#217068 - $15.00 USD Received 15 Jul 2014; revised 17 Oct 2014; accepted 20 Oct 2014; published 24 Oct 2014

$$FoM = \frac{\left(\alpha L_{eff}\right)^2 e^{2\alpha L}}{\Delta z \sqrt{N_{av} N_{phase}}} \frac{\sqrt{\delta \cdot \left(\Gamma_B / 2\pi\right)}}{\sigma_\nu} \tag{5}$$

Here α is the coefficient of linear propagation losses in the fiber under test and L_{eff} denotes its effective length. The form of Eq. (5) in [46] is more general: a couple of adaptions to the specific case of relatively short-reach B-OCDA were made above. Although FoM was primarily proposed for the study of long-reach B-OTDA setups, it was also used in [46] for the evaluation of high-resolution B-OTDA [10-11]. The experimental results of this work corresponds to FoM = 0.01 m^{-1}. This figure of merit is 1,000 times higher than that of the original phase-coded B-OCDA experiment reported in [15]. On the other hand, it is still an order of magnitude lower than those of high-resolution B-OTDA setups with comparable range and resolution (FoM = 0.1 and 0.2 m^{-1} for references [10] and [11], respectively [46]). The FoM of the results reported herein, as are those of all B-OCDA setups, is strongly compromised by the large number of position scans that are required for the analysis of the entire fiber. Although the number of scans, which equals the length of the Golomb code N_{phase} = 499 bits in this case, is orders of magnitude smaller than that of the original point-by-point B-OCDA, it remains much larger than that of high-resolution B-OTDA which requires only one or two scans [10-11]. Thus far, the benefit of the reported configuration in terms of smaller number of averages had not been sufficient to compensate for this inherent deficiency of B-OCDA.

Ongoing work is being dedicated to increasing the number of resolution points and to improving the figure of merit of the measurements, based on the following approaches: a) using shorter pulses in the amplitude modulation sequence, which would allow for closer spacing between correlation peaks and hence a smaller N_{phase}; b) employment of longer, more powerful amplitude modulation sequences to support the simultaneous interrogation of larger numbers of correlation peaks; c) increasing the average power of the pump beyond 100 mW; and (d) use of a polarization switch instead of the polarization scrambler, thereby reducing the necessary number of averages even further. With these potential advances, the interrogation of half-million resolution points in future works might become feasible.

Acknowledgments

Y. London, Y. Antman, R. Cohen and A. Zadok acknowledge the support of the Chief Scientist Office, the Israeli Ministry of Economics, through the KAMIN and MAGNETON programs.

#217068 - $15.00 USD Received 15 Jul 2014; revised 17 Oct 2014; accepted 20 Oct 2014; published 24 Oct 2014